J. Ocean Univ. China (Oceanic and Coastal Sea Research)
https://doi.org/10.1007/s11802-023-5449-0
ISSN 1672-5182, 2023 22 (5): 1313-1325
http://www.ouc.edu.cn/xbywb/
E-mail:xbywb@ouc.edu.cn

Mineralogical and Geochemical Constraints on the Mantle Source Characteristics of Basaltic Lavas from the Central Mariana Trough

LAI Zhiqing[1), 2)], GAO Wei[3), *], HAN Zongzhu[1)], GUO Kun[4)], ZHONG Shihua[1)], and ZHAO Guangtao[1), *]

1) *Key Laboratory of Submarine Geosciences and Prospecting Techniques*, *MOE and College of Marine Geosciences*, *Ocean University of China*, *Qingdao* 266100, *China*
2) *Key Laboratory of Marine Geology and Environment*, *Institute of Oceanology*, *Chinese Academy of Sciences*, *Qingdao* 266071, *China*
3) *National Deep Sea Center*, *Qingdao* 266237, *China*
4) *Center for Isotope Geochemistry and Geochronology*, *Pilot National Laboratory for Marine Science and Technology (Qingdao)*, *Qingdao* 266237, *China*

(Received December 27, 2021; revised April 15, 2022; accepted May 4, 2022)

Abstract The composition of mantle-derived basalts reflects the nature of their mantle source regions, which constrain magma generation and composition. Here we present a new whole rock major and trace elements and phenocryst composition of the basaltic lava in the central Mariana Trough. These data provide insights into the mantle source characteristics affected by subduction components. The rocks range from basalts to basaltic andesites, which have high subduction-mobile element contents (*e.g.*, K, U, Th, LREE) related to N-MORB. The calculated temperature and depth of magma generation are about 1300℃ and 30 km, respectively. Although the results above suggest that the addition of hydrous fluid and/or a melt derived from a slab decreases the temperature of mantle partial melting and mildly modifies the composition of a mantle source, the mantle source lithology from which primary magma is generated remains to be peridotite.

Key words backarc basin basalt; subduction component; mantle lithology; magma generation

1 Introduction

Chemical recycling in subduction zones, subduction inputs, and arc/backarc outputs has been a focused issue (Plank and Langmuir, 1998; Taylor and Martinez, 2003; Li *et al.*, 2021; Guo *et al*., 2022). The melting of mantle sources with multiple lithologies and physicochemical conditions, which may be affected by subduction components, is believed to be important in producing the range of magma compositions (Lambart *et al*., 2013; Doroozi *et al*., 2018; Yan *et al*., 2022). Identifying source mantle nature in the context of subduction zones is crucial for understanding the generation and evolution of mantle-derived magmas responsible for revealing the petrogenesis of igneous rocks.

The Mariana Trough is an actively extending backarc basin that is in crescent shape within the Philippine Sea Plate, beneath which the Pacific Plate is subducted (Lai *et al*., 2018). The spreading that forms the backarc basin occurs in the arc crust, which has been thinned through extension due to the subduction and rollback of the Pacific Plate (Anderson *et al*., 2017). The central Mariana Trough (CMT) backarc basin at 18°N is the widest, and the spreading axis is the farthest from the Mariana Trench with a maximum distance of 250 km, where no continental crust and minimal subducting components are introduced in the context of intraoceanic backarc basin (Gribble *et al.*, 1996; Zhao *et al.*, 2016). Therefore, the CMT is an ideal location to study element cycling and its relation to magmatism at the convergent margin.

The melting of a typically recycled oceanic crust and its reaction with a peridotite can produce an olivine-free pyroxenite at high pressure (Sobolev *et al*., 2007). Although reports have claimed that peridotites and basaltic lavas are exposed in the Mariana Trough and near regions (Ohara *et al.*, 2002; Li *et al*., 2021a), the lithologies and degrees of change for the physicochemical conditions of mantles affected by subduction components in the Mariana Trough are unclear. The compositions of these peridotites and basaltic lavas indicate that they derive from depleted MORB-type upper mantles with hydrous melts or fluid/mantle in-

* Corresponding authors. E-mail: gaowei@ndsc.org.cn
E-mail: gtzhao@ouc.edu.cn

teractions and relatively low partial melting temperatures (Gribble *et al.*, 1996; Tian *et al.*, 2010).

We focus on the lithologies, depths, and temperatures of the partial melting of mantle sources that is influenced by subduction components in the backarc spreading center. A combined approach involving petrology, mineralogy, and geochemistry is applied to this suite of rocks to constrain their source mantle nature. This study aims to understand mantle lithologies and physicochemical conditions in the Mariana Trough. We use these results to build a scenario that helps understand the mantle dynamic process in the backarc basin.

2 Geological Setting

The Izu-Bonin-Mariana (IBM) arc-trench system extends 2800 km and is a representative intra-oceanic convergent margin in the Western Pacific (Stern *et al.*, 1996). The rates that the Pacific Plate moved relative to the Mariana Trench vary from 16 mm yr^{-1} near the southern end (8°N, 137° 18′E) to 40 mm yr^{-1} near the northern end (23°30′N, 141° 30′E) (DeMets *et al.*, 2010). The West Mariana Ridge (WMR), Mariana Trough, Mariana Arc, and Mariana Trench are found in the Mariana subduction zones. WMR is a remnant arc. The Parece Vela Basin lies west of WMR, which used to be a backarc basin but now is extinct. The Mariana Arc is still in the post-arc expansion stage (Stern *et al.*, 2003). The Mariana Trough between WMR and Mariana Arc is a slow-spreading center with variable magmatic and hydro-thermal activity (Anderson *et al.*, 2017).

The Mariana Trough initiated spreading at 3–4 Myr (Stern *et al.*, 2003) and continues today with an increasingly opening rate of 15–45 mm yr^{-1} southward (Kato *et al.*, 2003). The Mariana Trough can be divided into three segments (Fig.1): the North Mariana Trough (NMT), CMT, and South Mariana Trough (SMT) (Pearce *et al.*, 2005; Ishibashi *et al.*, 2015). NMT (from 22°N to 24°N), in a rifting stage, narrows northward until the junction between the Mariana Arc and WMR at about 24°N (Ishibashi *et al.*, 2015). SMT (from 12.5°N to 17.6°N) narrows southward until 12.5°N (Pearce *et al.*, 2005). CMT (from 17.6°N to 21°N) has a mature spreading center where rift valleys generally develop (Masuda and Fryer, 2015). CMT between 20°N and 21°N, namely central Grabens, is formed through a magmatic extension during rifting (Stern *et al.*, 1996).

At 18°N, the spreading rate is 25 mm yr^{-1} (Kato *et al.*, 2003), and the crustal thickness is about 6 km (Bibee *et al.*, 1980; Sinton and Fryer, 1987). Mantle peridotite, basalt, andesite, dacite, and granite are exposed in this area (Hawkins *et al.*, 1990; Ohara *et al.*, 2002). Mariana Trough basalts are derived from a mixture of components from the subducting slab and the MORB-like mantle (Volpe *et al.*,

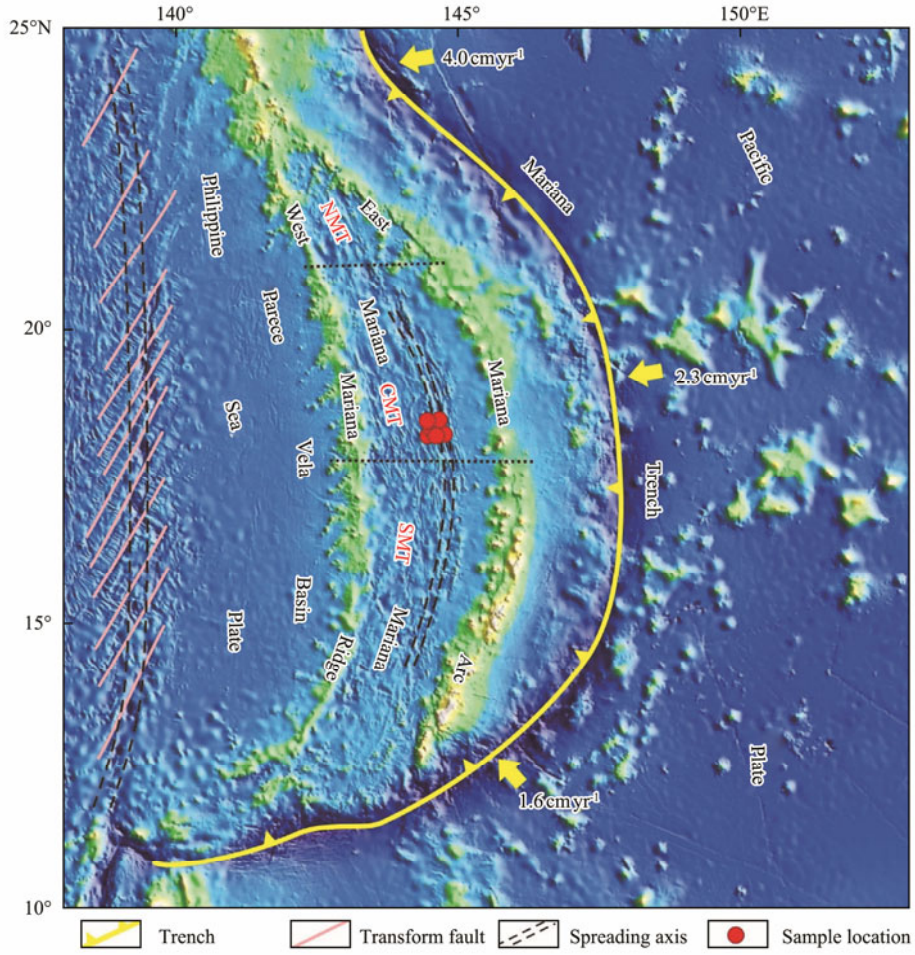

Fig.1 General tectonic map of the Mariana Trough and the location of samples (modified from Lai *et al.*, 2018). Subduction rates relative to the Philippine Plate are from DeMets *et al.* (2010).

1987; Tian *et al*., 2010; Li *et al*., 2021b). The proportion of subduction components also decreases southward and northward (Gribble *et al*., 1996, 1998; Zhao *et al*., 2016; Chen *et al*., 2021). Basalts dredged from CMT range between normal MORB-like and arc-like types (Volpe *et al*., 1987; Sano *et al*., 1998; Tian *et al*., 2010). A contrasting view that basalts are pure MORB-type has been stated (Sano *et al*., 1998; Gao *et al*., 2000). The low proportion and variation of SiO_2 contents in basaltic andesites are due to the fractional crystallization of plagioclase and olivine at low pressures (Hawkins *et al*., 1990; Lai *et al*., 2018).

3 Analytical Methods

Eight lavas were crushed and split. Clean rock fragments without weathering features were handpicked and cleaned with Milli-Q water. After drying at 50℃ with a drying cabinet, the fragments were leached with 0.1‰ HCl for two hours in an ultrasonic bath at 50℃. Then, all fragments were soaked in Milli-Q water for five days. The water was changed every eight hours to eliminate the influence of HCl on lavas. Ultimately, clean rock slabs cut from the central parts of lavas were used for thin section preparation. Others were ground into powder in an agate mortar before conducting a major and trace element analysis.

The major element chemical analysis was performed using a PANalytical-PW2424 X-ray fluorescence spectrometry on fused beads with the analysis accuracy estimated to be about 1% (relative) at the Australian Aoshi Mineral Analysis Laboratory (Guangzhou) Co., China. Standards SARM-45 were used to monitor analytical accuracy and precision. Trace elements were conducted at the Laboratory of Ocean Lithosphere and Mantle Geodynamic, Institute of Oceanology, Chinese Academy of Sciences. Trace elements were measured using an Agilent-7900 inductively coupled plasma mass spectrometer, following Chen *et al*. (2017). USGS standard materials BCR-2 and AGV-2 were used to monitor analytical accuracy and precision.

In situ major and trace elements for phenocrysts were determined on carbon-coated polished thin sections using a JXA-8230 electron probe micro-analyzer equipped with three WDS at the Key Laboratory of Submarine Geosciences and Prospecting Techniques, Ministry of Education, Ocean University of China in Qingdao, China. Detailed wavelength scans over standards were carried out prior to the analysis to select peak and background positions that would avoid interfering peaks from other elements present in the standards and samples. The operating conditions were 15 kV acceleration voltage, 20 nA beam current, and 2 μm beam diameter. Natural mineral and oxide standards were used for calibration, and ZAF correction procedures were applied (Lai *et al*., 2018). Calibration was based on the following standards: diopside (Si), olivine (Mg), almandine (Al), hematite (Fe), diopside (Ca), rutile (Ti), Cr-oxide (Cr), and Ni-oxide (Ni).

4 Results

All raw data of the studied basaltic lavas from CMT can be found in the following tables.

4.1 Petrography and Mineral Chemistry

Basaltic lavas have porphyritic and cryptocrystalline textures and are generally fine-grained with phenocrysts, microphenocrysts (> 100 mm), and microlites of olivine and plagioclase ± clinopyroxene. Plagioclase is the most abundant mineral phase (up to 80 vol.% of the crystal assemblage), followed by olivine (5 vol.%) and spinel (1 vol.%). Clinopyroxene occurs only locally in some samples (Fig.2). The groundmass is typical of clinopyroxene, olivine, plagioclase, and Fe-Ti oxides.

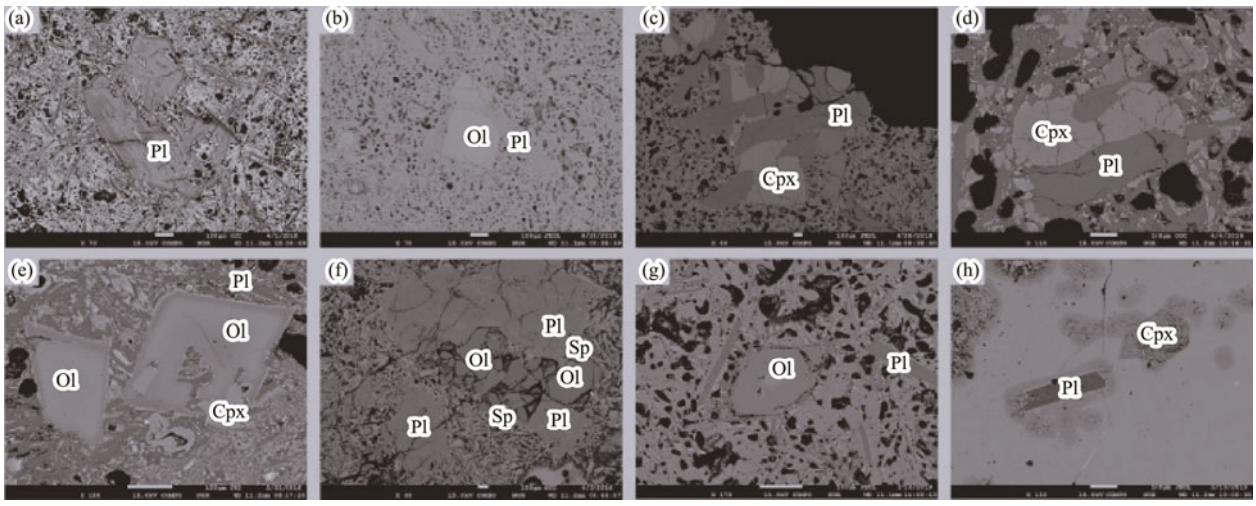

Fig.2 Back-scattered electron images of basaltic lavas. (a), plagioclase megacryst in sample L1-1; (b), olivine phenocryst and plagioclase microphenocryst in sample L1-2; (c), clinopyroxene and plagioclase microphenocryst in sample L2-1; (d), clinopyroxene and plagioclase phenocryst in sample L2-2; (e), olivine phenocryst with dissolved rim and clinopyroxene microlite in sample L3-1; (f), plagioclase megacryst, olivine and spinel phenocryst in sample L3-2; (g), olivine phenocryst and plagioclase microlite in sample L4-1; (h), clinopyroxene and plagioclase microlite in sample L4-2. Ol, olivine; Cpx, clinopyroxene; Pl, plagioclase; Sp, spinel; Gl, glass.

4.1.1 Olivine

Olivine phenocrysts are subhedral to euhedral and commonly show zonation. Some have sieved textures. Olivine compositions in the basaltic lavas from CMT are relatively uniform. SiO_2 contents vary from 40.38 wt.% to 41.45 wt.%, FeO contents from 9.71 wt.% to 13.97 wt.%, MgO contents from 47.05 wt.% to 49.46 wt.%, and CaO contents vary from 0.19 wt.% to 0.30 wt.%. NiO contents range from 0.15 wt.% to 0.30 wt.%, and Fo values from 78 to 90 (Table 1).

4.1.2 Spinel

Spinel is usually associated with olivine aggregates. Spinel composition in the basaltic rocks in CMT is different from that in depleted MORB mantles (Kamenetsky *et al*., 2001). FeO, MgO, Al_2O_3, TiO_2 contents and Cr# have the following ranges: 15.43–16.51 wt.%, 16.34–17.70 wt.%, 27.43–34.31 wt.%, 0.38–0.68 wt.%, and 0.39–0.49, respectively (Table 2).

Table 1 The dataset of representative olivine from basaltic lavas of CMT

Number (grain)	Sample	SiO_2	Al_2O_3	FeO	MnO	MgO	CaO	Cr_2O_3	NiO	Total	Fo
L1-1-OL1	L1-1	41.06	0.04	11.04	0.24	48.83	0.25	0.03	0.18	101.54	89
L1-1-OL2	L1-1	40.38	0.05	10.85	0.22	48.13	0.27	0.04	0.24	100.02	89
L2-1-OL1	L2-1	41.43	0.04	14.16	0.26	45.25	0.18	0.01	0.14	101.45	85
L2-1-OL2	L2-1	41.06	0.03	14.02	0.24	45.41	0.22	0.03	0.14	101.22	85
L2-1-OL3	L2-1	36.99	0.02	13.98	0.24	45.33	0.23	0.01	0.09	96.91	85
L2-1-OL4	L2-1	37.41	0.01	13.78	0.24	45.07	0.23	0.05	0.12	96.92	85
L2-1-OL5	L2-1	41.17	0.02	14.01	0.22	45.21	0.23	0.05	0.17	101.07	85
L2-1-OL6	L2-1	41.54	0.05	13.69	0.20	45.44	0.21	0.06	0.11	101.30	86
L2-2-OL1	L2-2	41.43	0.02	13.59	0.21	46.08	0.20	0.02	0.20	101.77	86
L2-2-OL2	L2-2	41.29	0.02	13.54	0.26	45.77	0.21	0.05	0.19	101.35	86
L2-2-OL3	L2-2	41.90	0.02	13.24	0.22	45.92	0.26	0.01	0.18	101.79	86
L2-2-OL4	L2-2	41.72	0.07	13.18	0.25	45.99	0.29	0.01	0.14	101.87	86
L2-2-OL5	L2-2	40.62	0.03	9.87	0.16	49.19	0.26	0.02	0.24	100.41	90
L3-1-OL1	L3-1	40.73	0.05	10.43	0.16	48.70	0.23	0.04	0.22	100.57	89
L3-1-OL2	L3-1	40.89	0.06	10.29	0.17	48.80	0.26	0.10	0.28	100.88	89
L3-1-OL3	L3-1	40.54	0.05	10.31	0.20	48.82	0.29	0.08	0.15	100.43	89
L3-1-OL4	L3-1	40.64	0.05	10.34	0.15	48.47	0.24	0.01	0.27	100.18	89
L3-1-OL5	L3-1	41.18	0.04	10.04	0.23	48.83	0.29	0.02	0.29	100.92	90
L3-1-OL6	L3-1	40.75	0.02	9.89	0.14	49.09	0.23	0.04	0.22	100.39	90
L3-2-OL1	L3-2	40.84	0.05	9.94	0.22	48.81	0.25	0.07	0.28	100.50	90
L3-2-OL2	L3-2	40.55	0.04	10.24	0.13	48.68	0.26	0.02	0.05	100.03	89
L3-2-OL3	L3-2	40.95	0.04	10.51	0.16	49.05	0.29	0.06	0.22	101.27	89
L3-2-OL4	L3-2	40.76	0.05	9.71	0.17	48.94	0.27	0.03	0.30	100.29	90
L3-2-OL5	L3-2	40.66	0.04	10.49	0.18	48.75	0.30	0.03	0.27	100.73	89
L3-2-OL6	L3-2	40.78	0.04	10.92	0.17	48.48	0.28	0.02	0.21	100.93	89
L3-2-OL7	L3-2	40.76	0.08	10.30	0.15	48.75	0.27	0.05	0.25	100.61	89
L4-1-OL1	L4-1	40.41	0.02	13.38	0.28	45.50	0.45	0.01	0.16	100.07	86
L4-1-OL2	L4-1	40.50	0.02	13.37	0.23	46.43	0.24	0.01	0.26	100.80	86
L4-1-OL3	L4-1	40.52	0.04	13.72	0.25	45.85	0.25	0.03	0.12	100.70	86
L4-1-OL4	L4-1	40.48	0.04	13.98	0.31	46.09	0.27	0.10	0.19	101.27	85
L4-1-OL5	L4-1	40.75	0.03	13.86	0.24	45.56	0.26	0.05	0.20	100.76	85
L4-1-OL6	L4-1	40.52	0.05	13.89	0.23	46.44	0.35	0.03	0.26	101.53	86
L4-2-OL1	L4-2	39.36	0.01	14.05	0.22	44.55	0.23	0.01	0.27	98.46	85
L4-2-OL2	L4-2	39.59	0.03	13.86	0.24	44.74	0.31	0.01	0.23	98.77	85
L4-2-OL3	L4-2	39.59	0.04	13.75	0.23	45.07	0.29	0.05	0.28	99.12	85
L4-2-OL4	L4-2	39.75	0.03	13.56	0.21	45.13	0.31	0.05	0.26	99.05	86
L4-2-OL5	L4-2	39.55	0.01	13.83	0.24	45.00	0.29	0.03	0.20	98.96	85
L4-2-OL6	L4-2	39.54	0.02	13.98	0.20	45.04	0.23	0.05	0.22	99.08	85

Table 2 The dataset of representative spinel from basaltic lavas of CMT

Number (grain)	Sample	SiO_2	Al_2O_3	FeO	MnO	MgO	CaO	Cr_2O_3	TiO_2	Sum	Cr#	Mg#
L1-1-Sp1	L1-1	0.07	29.08	16.00	0.18	16.68	0.07	37.75	0.52	100.37	0.47	0.65
L1-1-Sp2	L1-1	0.10	27.43	16.51	0.29	16.34	0.02	39.99	0.53	101.22	0.49	0.64
L3-2-Sp1	L3-2	0.09	34.31	15.43	0.23	17.70	0.04	32.85	0.38	101.04	0.39	0.67
L3-2-Sp2	L3-2	0.06	33.55	16.06	0.24	17.51	0.02	33.58	0.41	101.45	0.40	0.66
L3-2-Sp3	L3-2	0.05	32.85	15.81	0.23	17.22	0.05	34.14	0.42	100.79	0.41	0.66
L3-2-Sp4	L3-2	0.04	32.59	16.10	0.17	17.19	0.04	34.37	0.42	100.93	0.41	0.65
L3-2-Sp5	L3-2	0.04	31.95	15.64	0.28	17.25	0.07	34.64	0.40	100.29	0.42	0.66
L3-2-Sp6	L3-2	0.08	29.74	16.02	0.19	16.86	0.01	37.04	0.68	100.69	0.46	0.65
L3-2-Sp7	L3-2	0.06	29.08	15.51	0.22	16.76	0.09	37.37	0.55	99.65	0.46	0.66

4.1.3 Plagioclase

Plagioclases also appear in all samples, but their crystal sizes vary greatly. Most plagioclases are microlite. Megaphenocryst larger than 1000 μm is rare. Plagioclase phenocrysts have partial dissolution, sieve and oscillatory-zoned textures. Almost all megacrysts are fractured with dissolution and/or absorption. Plagioclases show a range of anorthite contents, varying from 64 to 90. An value of plagioclase edge and matrix plagioclase is commonly less than 70.

4.1.4 Clinopyroxene

Clinopyroxenes occur mainly as subhedral to euhedral prismatic and tabular crystals in the groundmass. A handful of clinopyroxenes are as huge (500 μm) as phenocrysts that commonly show zonation (Fig.2). Clinopyroxene compositions have the following ranges: 53.02–54.05 wt.% SiO_2, 5.84–6.26 wt.% FeO, 17.84–18.02 wt.% MgO, and 20.21–20.62 wt.% CaO.

4.2 Whole Rock Geochemistry

All samples are plotted on a total alkalis *versus* SiO_2 classification diagram for basalt and basaltic andesites (Fig.3). SiO_2 spans a slight range of SiO_2 contents of 49.44–52.61 wt.%. MgO contents vary between 4.89 and 8.10 wt.% with 50–69 Mg#, 8.87–12.35 wt.% CaO, and 0.91–1.48 wt.% TiO_2. Al_2O_3, CaO, and CaO/Al_2O_3 show much increase with increasing SiO_2 contents (Table 3). By contrast, Na_2O, SiO_2, K_2O, and P_2O_5 contents tend to decrease with increasing MgO contents. Compared with N-MORB (Sun and McDonough, 1989), these volcanic rocks have higher SiO_2, Al_2O_3, TiO_2, Na_2O, and CaO contents and significantly lower MgO, NiO, and CrO_2 contents, which resemble the major elements of Island Arc basalt (IAB) (Niu and O'hara, 2003). The studied lavas in CMT have a range of trace element contents. Zr, Ti, Nb, U, and Pb vary from 53.96×10^{-6} to 106.49×10^{-6}, 4828×10^{-6} to 8871×10^{-6}, 1.90×10^{-6} to 3.96×10^{-6}, 0.15×10^{-6} to 0.32×10^{-6}, and from 1.23×10^{-6} to 6.03×10^{-6}, respectively (Table 4). Sr, Pb, U, and K elements are enriched; Ta and Ti are depleted with respect to N-MORB. Primitive mantle-normalized trace element (Fig.4a) diagrams show the classic hallmarks of subduction magmatism, similar to IAB, with negative Nb-Ta and Ti anomalies and positive K, Pb, and Sr anomalies. These basaltic lavas have shallow-sloped chondrite-normalized REE abundance patterns, which exhibit slightly light rare earth element (LREE) enrichment and small negative Eu-anomalies (Fig.4b), with LREE/HREE, $(La/Yb)_N$, and $(Sm/Yb)_N$ ratios ranging from 2.05 to 2.54, 1.39 to 1.99, and 1.25 to 1.41, respectively. δEu values range from 1.03 to 1.12 with an average of 1.07.

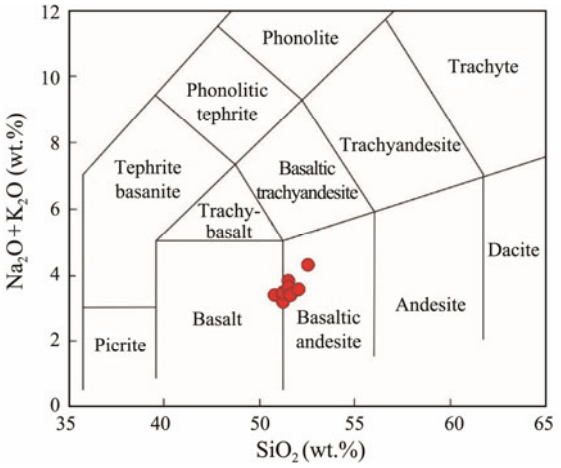

Fig.3 Total alkalis *vs.* SiO_2 classification diagram (Le Bas *et al*., 1986) for basaltic lavas.

Table 3 Major elements of basaltic lavas, composition, generation temperature and pressure of primary melts from CMT

Sample	L1-1	L1-2	L2-1	L2-2	L3-1	L3-2	L4-1	L4-2
Rock type	Basalt	Basaltic andesite	Basalt	Basaltic andesite	Basalt	Basalt	Basalt	Basalt
SiO_2	50.11	52.61	50.96	52.06	51.62	49.44	51.55	51.20
TiO_2	0.91	1.48	1.13	1.07	1.24	0.80	1.17	1.14
Al_2O_3	17.27	16.45	16.58	16.98	16.93	18.99	16.44	16.53
Cr_2O_3	0.04	0.01	0.03	0.01	0.03	0.04	0.02	0.02
FeOt	7.06	8.61	7.99	7.68	7.64	6.37	7.91	7.89
MnO	0.14	0.17	0.17	0.15	0.16	0.12	0.16	0.16
MgO	8.10	4.89	7.22	6.16	6.61	7.81	7.03	7.05
CaO	11.90	8.87	11.05	10.60	10.90	12.35	10.90	10.85
Na_2O	2.54	3.68	2.99	2.97	3.02	2.50	3.13	3.10
K_2O	0.38	0.68	0.46	0.60	0.49	0.31	0.47	0.36
P_2O_5	0.12	0.20	0.14	0.15	0.15	0.10	0.14	0.14
LOI	0.65	1.82	0.84	0.88	0.68	0.70	0.70	0.63
Cl	0.070	0.170	0.190	0.110	0.130	0.110	0.130	0.080
Total	99.29	99.64	99.75	99.42	99.60	99.64	99.75	99.15
Mg#	67.17	50.30	61.69	58.85	60.66	68.60	61.30	61.42
FC3MS	−0.48	−0.28	−0.43	−0.35	−0.38	−0.47	−0.41	−0.41
Fe/Mn	50.59	50.85	47.19	51.37	47.93	53.30	49.63	49.51
H_2O[a]	1.00	1.00	1.00	1.00	1.00	1.00	1.00	1.00
Temperature[b] (℃)	1276	1346	1314	1298	1297	1247	1308	1309
Pressure[c] (GPa)	1.0	1.3	1.2	1.0	1.1	0.9	1.1	1.1
Pressure[c] (GPa)	1.1	1.3	1.3	1.0	1.0	1.2	1.1	1.1

Notes: [a] Water contents after Newman *et al*. (2000); [b] Temperature and pressure for generation of primary melts calculated after Lee *et al*. (2009); [c] Pressure for generation of primary melts calculated after Scarrow and Cox (1995).

Table 4 Trace elements of basaltic lavas from CMT

Sample	L1-1	L1-2	L2-1	L2-2	L3-1	L3-2	L4-1	L4-2
Rock type	Basalt	Basaltic andesite	Basalt	Basaltic andesite	Basalt	Basalt	Basalt	Basalt
Sc	32.60	32.27	33.72	34.66	32.46	28.43	35.10	34.15
V	210.52	306.80	243.31	259.71	251.05	179.25	251.35	239.31
Cr	244.26	23.17	190.67	67.70	215.09	258.03	155.99	157.26
Co	32.19	27.94	32.23	28.66	29.58	30.51	32.27	31.61
Ni	291.70	131.66	171.46	145.91	462.63	292.08	228.70	429.78
Zn	60.69	73.75	66.93	64.44	65.20	49.49	70.43	69.77
Ga	13.53	16.60	14.41	14.88	15.03	13.23	14.76	14.49
Rb	4.85	8.05	5.81	8.03	4.97	3.22	5.29	4.72
Sr	211.37	221.08	188.56	233.90	178.46	202.74	185.66	191.26
Y	19.03	29.48	23.83	22.39	25.67	16.67	25.12	23.69
Zr	1.69	2.76	2.12	1.95	2.32	1.41	2.25	2.11
Nb	1.90	3.96	2.42	2.56	3.00	1.90	2.68	2.49
Cs	0.08	0.16	0.16	0.15	0.08	0.05	0.09	0.09
Ba	47.88	68.98	35.10	61.21	34.98	28.44	40.41	50.99
Hf	1.69	2.76	2.12	1.95	2.32	1.41	2.25	2.11
Ta	0.12	0.25	0.16	0.17	0.20	0.12	0.18	0.16
W	0.07	0.09	0.08	0.07	0.07	0.06	0.09	0.07
Pb	1.98	1.74	3.24	1.23	1.34	1.35	3.93	6.03
Th	0.38	0.71	0.37	0.68	0.40	0.27	0.38	0.36
U	0.17	0.32	0.18	0.24	0.19	0.15	0.15	0.16
La	4.45	7.63	4.90	6.30	5.01	3.33	4.88	4.72
Ce	10.71	18.57	12.26	14.69	13.02	8.40	12.92	12.10
Pr	1.66	2.79	1.97	2.20	2.05	1.32	2.04	1.92
Nd	7.83	12.80	9.25	10.05	9.67	6.29	9.74	9.22
Sm	2.35	3.72	2.82	2.86	2.91	1.90	3.01	2.83
Eu	0.94	1.43	1.14	1.13	1.16	0.81	1.20	1.16
Gd	3.05	4.78	3.77	3.69	4.08	2.59	3.99	3.76
Tb	0.54	0.82	0.67	0.63	0.71	0.46	0.69	0.66
Dy	3.43	5.20	4.23	4.03	4.55	3.00	4.46	4.29
Ho	0.74	1.11	0.92	0.85	0.96	0.64	0.97	0.90
Er	2.09	3.16	2.65	2.47	2.80	1.80	2.78	2.59
Tm	0.30	0.47	0.38	0.36	0.41	0.27	0.41	0.38
Yb	1.92	2.94	2.40	2.27	2.58	1.69	2.50	2.39
Lu	0.30	0.47	0.38	0.35	0.41	0.26	0.40	0.37
LREE/HREE	2.26	2.48	2.10	2.54	2.05	2.06	2.09	2.08
(La/Yb)N	1.66	1.86	1.47	1.99	1.39	1.42	1.40	1.42
(Sm/Yb)N	1.36	1.41	1.31	1.40	1.25	1.26	1.34	1.31
Ce/Ce*	0.99	1.02	0.99	1.00	1.02	1.00	1.02	1.00

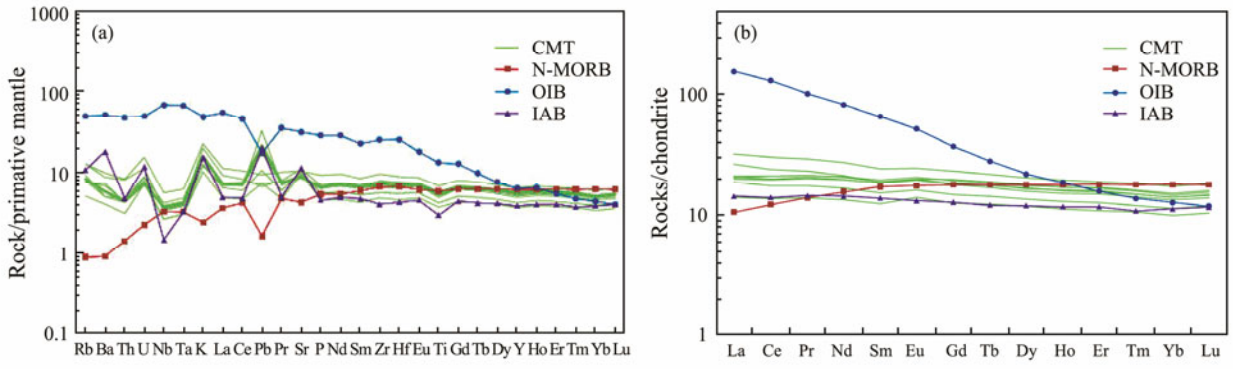

Fig.4 (a) REE patterns normalized by chondrites. (b) Multielement diagrams normalized by the primitive mantle. Normalization, N-MORB, and OIB values are from Sun and McDough (1989). IAB is from Niu and O'hara (2003).

5 Discussion

5.1 Post-Magmatic Alteration

Loss on ignition (LOI) is usually used to quantitatively reveal the degree of rock alteration. The LOI of all samples in CMT is from 0.63 to 1.82, with an average value of 0.86. The submarine alteration can alter K, U, Rb, Cs, and Cl element contents strongly (Pearce and Norry, 1979). More-

over, Ce^{4+} is more stable than other trivalent rare earth elements during the rock alteration process, which makes rocks exhibit obvious Ce deletion (Ce/Ce* <0.8, Ce/Ce* = $Ce_N/(La_N \times Nd_N)^{0.5}$) (Hart and Staudigel, 1982; Le Roux *et al*., 2010). The Ce/Ce* values of basaltic lavas in CMT range from 0.99 to 1.02 without an obvious anomaly. This, combined with the poor correlation between LOI and Rb, K_2O, Cl/K, and Ce/Ce* (Fig.5), collectively suggests that the change of LOI is not an imprint of rock alteration. A high alteration degree of rocks has great Cl/K ratios (Marschall *et al*., 2017). Cl/K does not show a good correlation with Ce/Ce*. Therefore, the relatively low LOI contents and variations in samples may be results of the enrichment of elements migrated from subducted slabs, such as K, Rb, and Pb and H_2O content. In a word, basaltic lavas in CMT have undergone no or only slight submarine alterations.

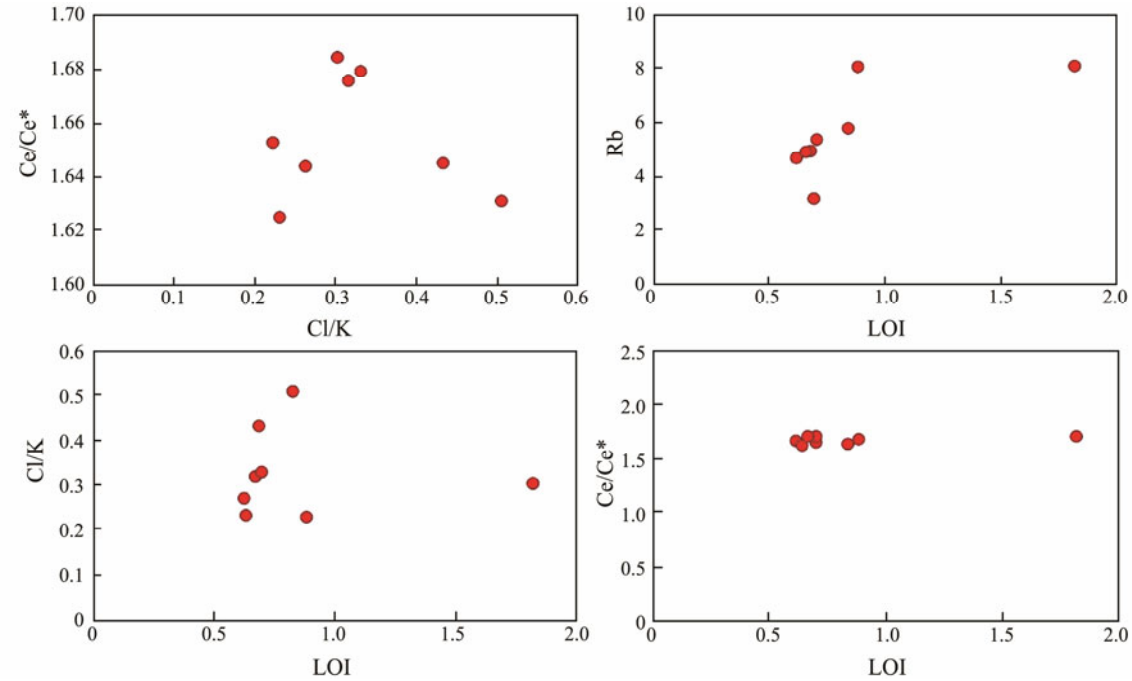

Fig.5 Correlation between LOI and different contents that are sensitive to alteration for basaltic lavas.

5.2 Role of Subduction Components

To some extent, backarc basin basalts (BABB) can usefully be the products of water-rock reaction between mantles and the influx of subduction components (Gribble *et al*., 1996; Pearce *et al*., 2005; Zhang *et al*., 2019; Li *et al*., 2022). Mantle components are significantly depleted in subduction-immobile elements, such as Nb, Ta, Zr, Hf, Ti, and HREE. Subduction components (fluids/melts) from subducted slabs are usually rich in subduction-mobile elements, such as K, Rb, Sr, Ba, U, Th, and Pb (Stern *et al*., 2003). Therefore, the influence of subduction components on backarc basin magmatism can be identified on the basis of the compatibility and migration of subduction-immobile and -mobile elements (Taylor and Martinez, 2003; Pearce *et al*., 2005).

The Rb, Sr, K, U, Pb, and LREE elements with positive anomalies in the standardized diagram of primitive mantles for trace elements in basaltic lavas from CMT are significantly higher than those in N-MORB, lower than OIB and similar to IAB (Fig.4a). The depleted high-field strength elements (*e.g*., Nb, Ta, Ti, and HREE) have similar characteristics to N-MORB. This is a typical trace element distribution pattern of BABB and IAB affected by subduction components (Niu and O'Hara, 2003; Pearce *et al*., 2005; Yan *et al*., 2019). Compared with MORB with Al_2O_3 15.13, TiO_2 1.53, TiO_2/K_2O 10.93, and $^{87}Sr/^{86}Sr$ 0.702819 (Gale *et al*., 2013), the basaltic lavas from CMT have higher Al_2O_3 contents with an average of 16.20, $^{87}Sr/^{86}Sr$ with an average of 0.703143 (Zhao *et al*., 2016), lower TiO_2 contents with an average of 1.06, and TiO_2/K_2O ratio with an average of 2.08. In general, the high Al_2O_3, K_2O and low TiO_2 contents in BABB are related to the addition of subduction components that contain subduction-mobile elements (Pearce *et al*., 2005). If the enrichment of large ion lithophile elements in the basaltic lavas from CMT is caused by fractional crystallization, then more than 60% of basic minerals need to be crystallized and separated, inconsistent with the characteristics of basaltic lavas undergoing the low-degree separation crystallization process (Hawkins and Melchior, 1985; Lai *et al*., 2018). Basaltic lavas have high contents of Mg#, Cr, and Ni in the whole rock, and MgO has no good correlation with K_2O. Therefore, the magmatism in CMT may not undergo a high degree of fractional crystallization and is affected by subduction components (Volpe *et al*., 1987).

The chondrite-normalized REE diagram shows nearly identical sloped patterns relative to IAB, LREE enrichment and small negative Eu-anomalies (Fig.4b) with slightly high LREE/HREE, $(La/Yb)_N$ and $(Sm/Yb)_N$ ratios, indicating that magma generation and/or evolution are influenced by subduction components. The high values of La/Nb (1.94–

2.78), La/Ta (25–39.94), and Zr/Nb (26.91–32.77) ratios, coupled with Sr-Nd isotope ratios in the studied rocks (Zhao *et al*., 2016; Yan *et al*., 2019), also possibly indicate the influences of subduction components. In addition, spinel in abyssal peridotites usually contains low or negligible amounts (< 0.25 wt%) of TiO_2 (Kamenetsky *et al*., 2001). Therefore, spinel in basaltic lavas in CMT that has high TiO_2 content with 0.38%–0.68% is attributed to reactions with impregnating melts enriched with subduction-mobile elements.

5.3 Mantle Source Lithology

The subduction and recycling of oceanic crust into the low mantle depth can produce pyroxenites to form a 'marble cake model' (Allègre and Turcotte, 1986; Sobolev *et al*., 2007). The characteristics of major and trace element contents in the basaltic melts from the pyroxenite mantles are obviously distinct from those from the peridotite mantles (Yang and Zhou, 2013; Li *et al*., 2021a). Basalts that are the products of mantle partial melting can be used as a probe to decipher the nature of mantles (Zhang *et al*., 2012, 2020; Xu *et al*., 2020). However, the composition of basalts has evolved and varied owing to fractionation crystallization. The primitive melt of basalts is necessary to be backtracked to identify mantle lithology.

We determine primary magma compositions using PRIMELT3 to avoid the effects of olivine fractionation for basaltic lavas in CMT (Herzberg and Asimow, 2015). The CaO *versus* MgO and Fe/Mn diagrams (Fig.6) doubtlessly do not discriminate mantle source lithology. Some basaltic lavas and primitive melts plot within the area of pyroxenite partial melts or near the boundary between pyroxenite and peridotite partial melts. The Fe/Mn ratio of melts derived from the partial melting of pyroxenites is higher (>50) than that of the melts of peridotites (Pertermann and Hirschmann, 2003). The Fe/Mn ratio of basaltic lavas in CMT is about 50, which also does not identify lithology. The most unrecognizable reason above is that PRIMELT3 only avoids the effects of olivine fractionation for basaltic lavas but considers the effects of clinopyroxene and plagioclase fractionation. This fractionation from melts can increase Fe/Mn ratios and decrease CaO contents (Wang *et al*., 2012). The negative correlation between Fe/Mn ratios and MgO contents and positive correlation between CaO and MgO contents (Fig.7) suggest that clinopyroxene and plagioclase fractionation takes place and changes basaltic lava valves (Lai *et al*., 2018). Therefore, basaltic lavas have relatively low Fe/Mn ratios of 47.19–53.30, suggesting that primitive melts are not possible from pyroxenite partial melts. ΔNb (ΔNb = 1.74 + log(Nb/Y) − 1.92log(Zr/Y)), from −0.25 to −0.18, moreover, indicates that they cannot be derived from pyroxenites (Fitton *et al*., 1997).

To reduce the fractional crystallization influence on the whole rock composition of basaltic lavas, diagrams for FC3-MS *versus* major element contents are introduced to accurately identify mantle lithology in CMT (Yang and Zhou, 2013). Melts derived from peridotite mantles have low FC3MS (<0.65), whereas melts derived from pyroxenite

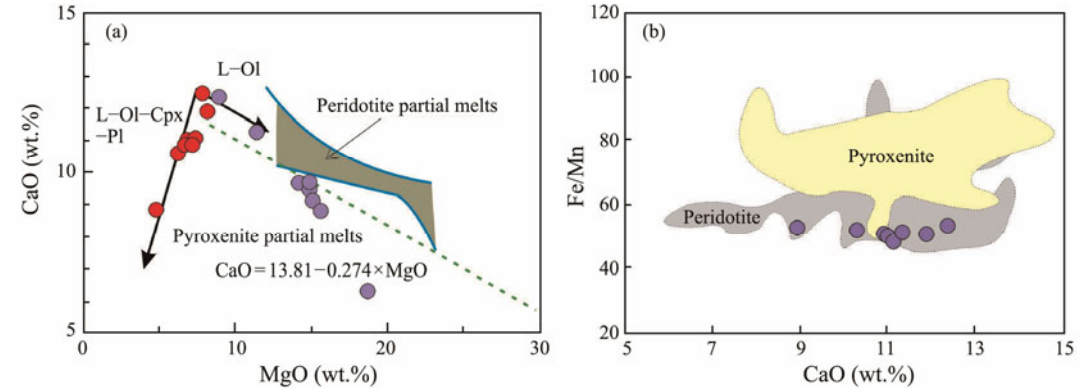

Fig.6 CaO *vs*. MgO and Fe/Mn diagrams for basaltic lavas and primary melts. (a) The green line and the shaded area for peridotite partial melts are from Herzberg and Asimow (2008). Red plots are basaltic lavas. (b) Areas for peridotite and pyroxenite partial melts are after Liu *et al*. (2008). Purple plots are primary melts calculated using PRIMELT3 MEGA.XLSM software (Herzberg and Asimow, 2015).

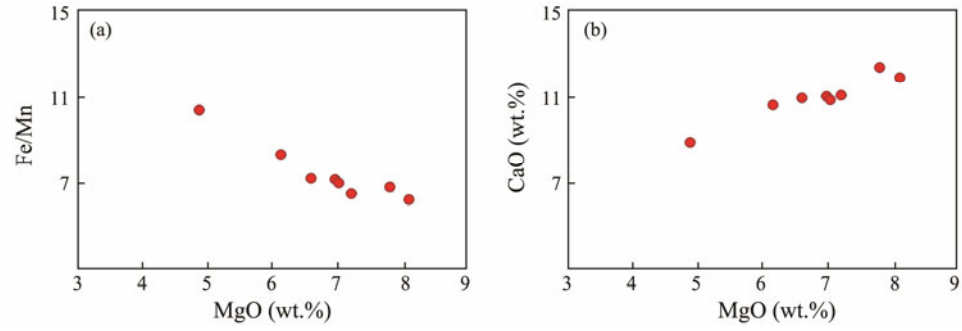

Fig.7 Plots of MgO *vs*. Fe/Mn and CaO of basaltic lavas.

mantles tend to be high (Yang and Zhou, 2013). FC3MS values of basaltic lavas in CMT vary from −0.48 to −0.28. As illustrated in the diagrams of FC3MS *versus* MgO and Na_2O+K_2O (Fig.8), all basaltic lavas from CMT are located in the peridotite mantle field and far from the pyroxenite mantle field.

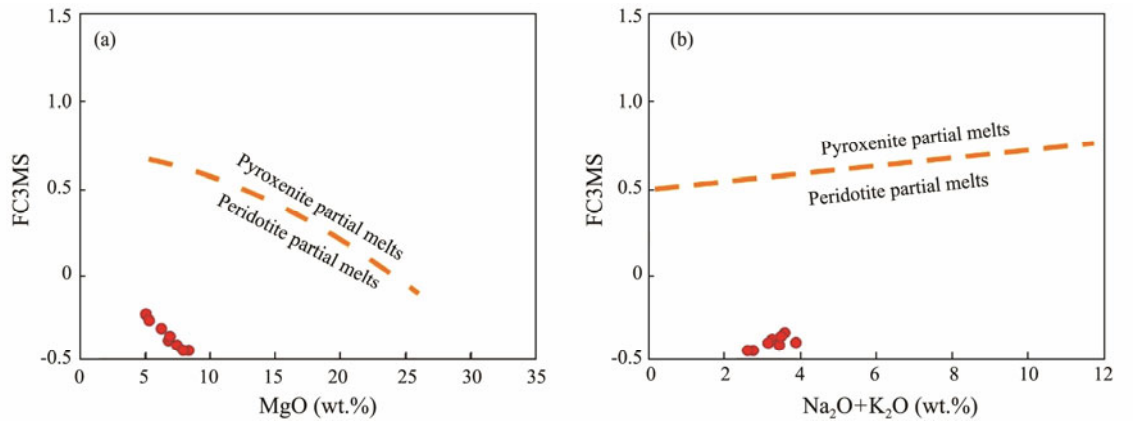

Fig.8 Diagrams showing FC3MS ($FC3MS=FeOT/CaO-3\times MgO/SiO_2$) *vs.* MgO (a) and Na_2O+K_2O (b). The orange line is from Yang and Zhou (2013).

Basaltic magma in CMT transfers rapidly from the depth beneath Moho to the surface (Lai *et al*., 2018). Vestiges of polythermal fractional crystals (olivine, plagioclase, and spinel) are preserved in these basaltic lavas. Olivine is a preferential phenocryst at the beginning of fractional crystallization, compared with the whole rock composition, which can be used to well determine the source mantle nature. Ni contents range from 1162×10^{-6} to 2349×10^{-6}, with a weighted mean of $(1866\pm290)\times10^{-6}$ in olivine in basaltic lavas, which is far less than that in olivine derived from the pyroxenite mantle source ($>4000\times10^{-6}$, Fo, 90) (Herzberg, 2011). The Ca contents range from 1860×10^{-6} to 3030×10^{-6}, with a weighted mean of $(2590\pm287)\times10^{-6}$, which is higher than that in olivine derived from the pyroxenite mantle source ($<1700\times10^{-6}$) (Herzberg, 2011). In the diagrams of Fo *versus* Cr and 100×Mn/Fe *versus* Ni (Fig.9), basaltic lavas are almost entirely plotted in the peridotite mantle field.

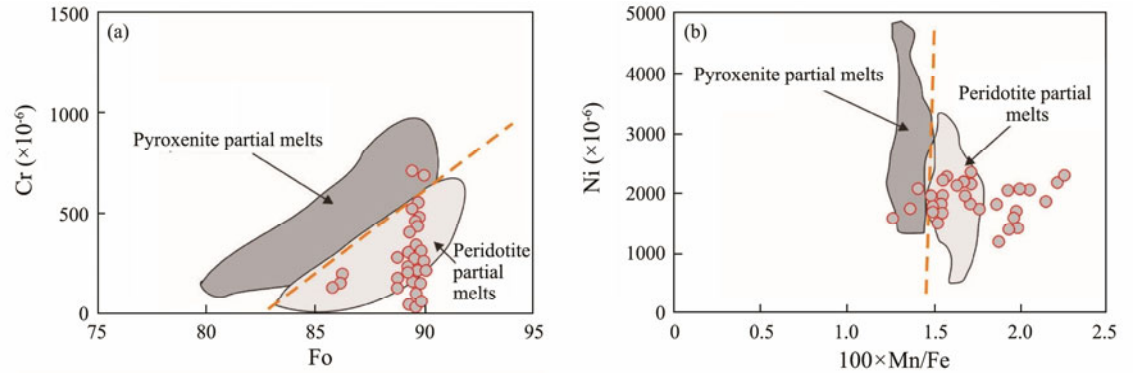

Fig.9 Cr *vs.* Fo (a) and Ni *vs.* 100×Mn/Fe (b) in olivine phenocrysts from basaltic lavas. The orange line and shade areas are from Herzberg (2011) and Sobolev *et al*. (2007).

Cr-spinel is a common accessory mineral in most types of primitive high Mg# volcanic rocks; it is considered an important petrological indicator of source mantle nature (Nekrylov *et al*., 2018; Li *et al*., 2021a). A high Mg#, from 67 to 69, of spinel in basaltic lavas is slightly lower than that in fore-arc peridotites at a given Cr# (Arai and Ishimaru, 2007). The chromian spinel falls almost entirely within the abyssal peridotite field (Fig.10a). The TiO_2 *versus* Al_2O_3 diagram for primitive spinel compositions, when olivine Fo >84, can discriminate geodynamic settings (Kamenetsky *et al.*, 2001). In this diagram, spinel compositions from CMT fall into the MORB field (Fig.10b). To sum up, the mantle source lithology in CMT, where primary magmas are generated, is peridotite.

5.4 Source Mantle Conditions

Primary magma compositions are usefully constrained by physical and chemical source mantle properties (Herzberg and Asimow, 2015). Decoding the temperatures and depths of partial mantle source melting is important to constrain the magma genesis and petrogenesis of volcanic rocks (Herzberg, 2011).

In Fig.11, the temperatures and pressures of mantle source melting are determined using Visual Basic Excel Code, based on whole rock composition (Lee *et al*., 2009). The latter method produces low temperatures due to the intro-

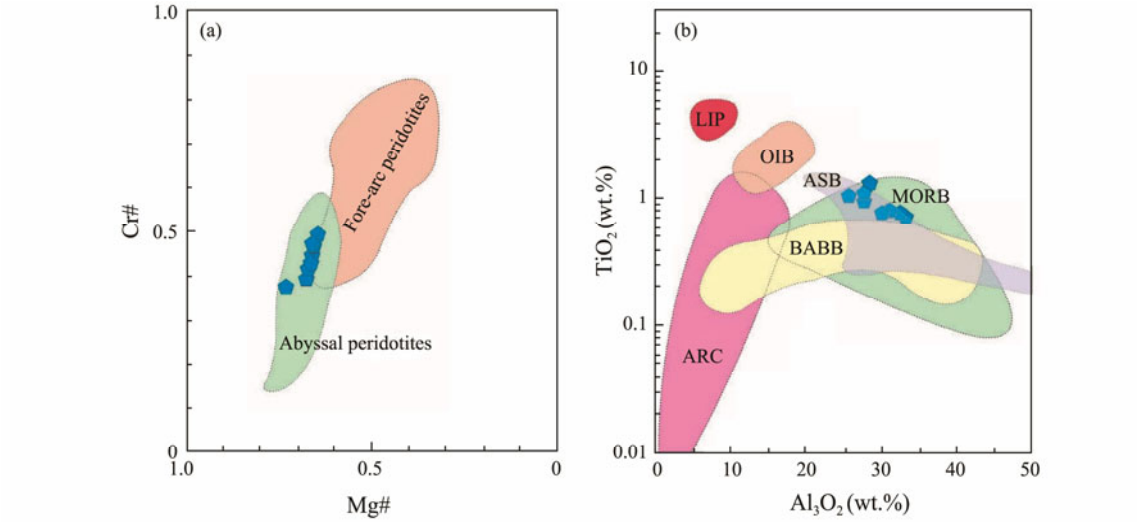

Fig.10 TiO_2 *vs.* Al_2O_3 and Cr# *vs.* Mg# diagrams for chromian spinel. Fields of typical spinel compositions for MORBs, BABBs, LIPs, ARCs, and OIBs are from Kamenetsky *et al*. (2001), abyssal peridotites and fore-arc peridotites are from Arai *et al*. (2007), and peridotites from the Amami Sankaku Basin (ASB) are from Li *et al*. (2021a).

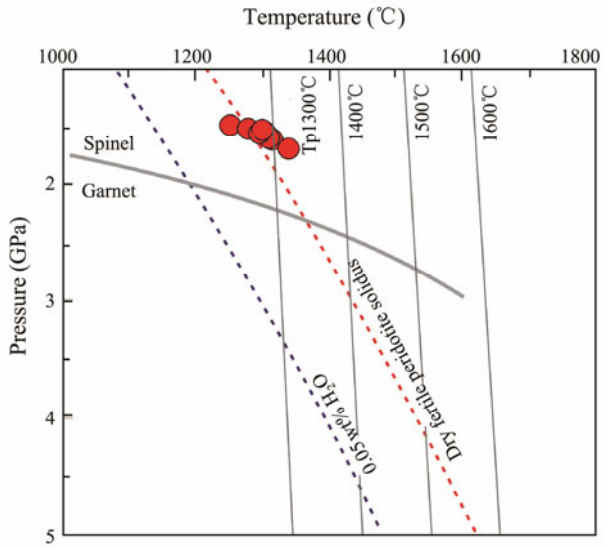

Fig.11 Pressure and temperature estimates (using thermobarometer of Lee *et al*., 2009) of primary magma generation beneath CMT.

duction of water contents and oxygen fugacity for calculations. The calculated melting temperatures and pressures vary from 1247 to 1314℃ and from 0.9 GPa to 1.3 GPa, respectively. These temperatures are slightly cooler than the ambient mantle temperatures of upper mantle sources beneath MOR with 1454℃±81℃ (Putirka *et al*., 2007). The reason for low temperatures above for basaltic lavas in CMT is attributed to the addition of subduction components in source mantle regions. The water and/or aqueous melts from the dehydration and/or partial melting of subducting slab decrease the temperature of the partial melting of mantle wedge.

In comparison with the calculated pressures above, the depths of primary magma generation can be estimated using the major oxides of primitive melts. A linear regression equation [P (kbar)=213.6−4.05×SiO_2] can calculate pressure with SiO_2 contents (Scarrow and Cox, 1995). This equation leads to estimates of apparent magma segregation pressures from 1.0 GPa to 1.3 GPa. According to these estimates, the primary magmas are generated at about 25–36 km by assuming a crustal density of 2800 kg m^{-3} and upper mantle density of 2972 kg m^{-3} (Mariita and Keller, 2007; Tenzer *et al*., 2013). The estimated magma generation depth suggests that primary magmas in CMT are segregated from the upper mantle below the Moho, whose depth is 6 km (Bibee *et al*., 1980). A similar generation depth in Amami Sankaku Basin (0.7–2.0 GPa), which is the oldest remnant arc of IBM, and in the Mariana Trough (0.5–1.0 GPa) has been proposed (Sinton and Fryer, 1987; Li *et al*., 2021a).

5.5 Geodynamic Implications

Previous studies favored the depleted MORB-type mantle as the main source for primary magmas beneath the Mariana Trough with the addition of subduction components (Volpe *et al*., 1987; Tian *et al*., 2010; Zhao *et al*., 2016). Our study on basaltic lavas, however, indicates that only peridotites play a role in the origin of basaltic melts in CMT. The role of pyroxenites is scarce or indistinct. Here, we attempt to discuss the mantle evolution and process that result in the geochemistry of basaltic lavas.

Chemical components from subducted slabs into mantle wedges modify mantle compositions and conditions and trigger melting at relatively lower temperatures than normal (Stern *et al*., 2003; Zhang *et al*., 2021). Our results of low calculated temperatures of partial melting are lower than those beneath MOR, suggesting that the addition of hydrous fluids and/or melts from slab decreases the melting temperatures in mantle sources. The primary magma generation is at depths of less than 50 km, whereas the Pacific Plate subducts at depths of >100 km beneath the Mariana Arc, at a great depth (>200 km) beneath the Mariana Trough (England *et al*., 2004). In subduction zones,

sediments generally dehydrate first (at depths of 50 km), then oceanic crust (at depths of 100–200 km), and finally serpentinized mantles (at depths of 150–250 km) (Rüpke *et al*., 2004). To some extent, the subduction of slabs and opening of backarc basins have greatly modified upper mantle compositions by slab-derived melts/fluids. The melting of a typically recycled oceanic crust at high pressure (P> 3.0 GPa) and the reaction of this melt with peridotites produce olivine-free pyroxenites (Sobolev *et al*., 2005). Nonetheless, primary magma generation in CMT is only at depths of 25–36 km, which is shallower than the formation depths of pyroxenites in subduction zones. The derivation of basaltic lavas in the Mariana Trough involves the enrichment of incompatible elements during some metasomatic events prior to partial melting (Sinton and Fryer, 1987). Hence, the mantle source lithology here involves peridotites that are also distributed at the backarc side of the arc (Arai *et al*., 2007). However, ascertaining whether pyroxenites exist at great depths (even>100 km), from which hydrous fluids and/or melts derive or pass through, is difficult.

Therefore, we speculate that hydrous fluids and/or melts are derived from the subducted Pacific Plate at levels deeper than 50 km, ascend through upper mantle while attaining chemical equilibrium with mantle wedge, and then facilitate the partial melting of mantle and produce primary magmas with low partial melting temperatures at depths of 25–36 km in CMT.

6 Conclusions

To investigate mantle source lithologies and conditions in the CMT introduced by subduction components, major and trace element concentrations of whole rocks and phenocrysts from basaltic samples are analyzed. Our interpretations of these data show the following:

1) Volcanic rocks are basalts and basaltic andesites that are significantly depleted in subduction-immobile elements, such as Nb, Ta, Ti, and HREE, and rich in subduction-mobile elements, such as K, Rb, Sr, U, and Pb.

2) Melting temperatures and pressures for primary magmas are 1247–1314℃ and 0.9–1.3 GPa, respectively. Aqueous fluids and/or hydrous melts from the dehydration and/or partial melting of subducting slabs decrease the melting temperatures of mantles. However, the mantle source lithology where primary magmas are generated remains to be peridotites.

3) Hydrous fluids and/or melts are first derived from the subducted Pacific Plate at levels deeper than 50 km and then facilitate the partial mantle melting and primary magma generation at depths of 25–36 km in CMT.

Acknowledgements

This work was financially supported by the Shandong Provincial Natural Science Foundation, China (Nos. ZR2017PD002 and ZR2019BD010), the Open Fund of the Key Laboratory of Marine Geology and Environment, Chinese Academy of Sciences (Nos. MGE2019KG05 and MGE2021KG01), the Fundamental Research Funds for the Central Universities (No. 202051009). Drs. Xiaohong Wang, Pu Sun, Meng Duan, and Pengyuan Guo are appreciated for their laboratory assistance.

References

Allègre, C. J., and Turcotte, D. L., 1986. Implications of a two-component marble-cake mantle. *Nature*, **323** (6084): 123-127.

Anderson, M. O., Chadwick, W. W., Hannington, M. D., Merle, S. G., Resing, J. A., Baker, E. T., *et al*., 2017. Geological interpretation of volcanism and segmentation of the Mariana back-arc spreading center between 12.7°N and 18.3°N. *Geochemistry, Geophysics, Geosystems*, **18** (6): 2240-2274.

Arai, S., Abe, N., and Ishimaru, S., 2007. Mantle peridotites from the Western Pacific. *Gondwana Research*, **11** (1): 180-199.

Arai, S., and Ishimaru, S., 2007. Insights into petrological characteristics of the lithosphere of mantle wedge beneath arcs through peridotite xenoliths: A review. *Journal of Petrology*, **49** (4): 665-695.

Bibee, L. D., Shor, G. G., and Lu, R. S., 1980. Inter-arc spreading in the Mariana Trough. *Marine Geology*, **35** (1): 183-197.

Chen, S., Wang, X. H., Niu, Y. L., Sun, P., Duan, M., Xiao, Y. Y., *et al*., 2017. Simple and cost-effective methods for precise analysis of trace element abundances in geological materials with ICP-MS. *Science Bulletin*, **62** (4): 277-289.

Chen, Y. H., Niu, Y. L., Xue, Q. Q., Gao, Y. J., and Castillo, P., 2021. An iron isotope perspective on back-arc basin development: Messages from Mariana Trough basalts. *Earth and Planetary Science Letters*, **572**: 117133.

DeMets, C., Gordon, R. G., and Argus, D. F., 2010. Geologically current plate motions. *Geophysical Journal International*, **181** (1): 1-80.

Doroozi, R., Vaccaro, C., Masoudi, F., and Petrini, R., 2018. Petrogenesis and mantle source characteristics of Triassic alkaline basaltic rocks of North Kamarbon, northern central Alborz, Iran. *Solid Earth Sciences*, **3** (4): 115-129.

England, P., Engdahl, R., and Thatcher, W., 2004. Systematic variation in the depths of slabs beneath arc volcanoes. *Geophysical Journal International*, **156** (2): 377-408.

Fitton, J. G., Saunders, A. D., Norry, M. J., Hardarson, B. S., and Taylor, R. N., 1997. Thermal and chemical structure of the Iceland plume. *Earth and Planetary Science Letters*, **153** (3): 197-208.

Gale, A., Dalton, C. A., Langmuir, C. H., Su, Y., and Schilling, J. G., 2013. The mean composition of ocean ridge basalts. *Geochemistry, Geophysics, Geosystems*, **14** (3): 489-518.

Gribble, R. F., Stern, R. J., Bloomer, S. H., Stüben, D., O'Hearn, T., and Newman, S., 1996. MORB mantle and subduction components interact to generate basalts in the southern Mariana Trough back-arc basin. *Geochimica et Cosmochimica Acta*, **60** (12): 2153-2166.

Gribble, R. F., Stern, R. J., Newman, S., Bloomer, S. H., and O' Hearn, T., 1998. Chemical and isotopic composition of lavas from the northern Mariana Trough: Implications for magmagenesis in back-arc basins. *Journal of Petrology*, **39** (1): 125-154.

Guo, K., Wang, X. Y., Chen, S., Shang, L. N., Liu, B. Q., Zhang, X., *et al*., 2022. The delamination of lower crust in continental back-arc basin: Evidence from Sr isotope and elemental compositions of plagioclase and clinopyroxene in andesites from Kueishantao, North of Taiwan, China. *Lithos*, **416-417**: 106653.

Hart, S. R., and Staudigel, H., 1982. The control of alkalies and uranium in seawater by ocean crust alteration. *Earth and Planetary Science Letters*, **58** (2): 202-212.

Hawkins, J. W., and Melchior, J. T., 1985. Petrology of Mariana Trough and Lau Basin basalts. *Journal of Geophysical Research: Solid Earth*, **90** (B13): 11431-11468.

Hawkins, J. W., Lonsdale, P. F., Macdougall, J. D., and Volpe, A. M., 1990. Petrology of the axial ridge of the Mariana Trough backarc spreading center. *Earth and Planetary Science Letters*, **100** (1): 226-250.

Herzberg, C., 2011. Identification of source lithology in the Hawaiian and Canary Islands: Implications for origins. *Journal of Petrology*, **52** (1): 113-146.

Herzberg, C., and Asimow, P. D., 2008. Petrology of some oceanic island basalts: PRIMELT2.XLS software for primary magma calculation. *Geochemistry, Geophysics, Geosystems*, **9**: Q09001, DOI: 10.1029/2008GC002057.

Herzberg, C., and Asimow, P. D., 2015. PRIMELT3 MEGA.XLSM software for primary magma calculation: Peridotite primary magma MgO contents from the liquidus to the solidus. *Geochemistry, Geophysics, Geosystems*, **16** (2): 563-578.

Ishibashi, J. I., Tsunogai, U., Toki, T., Ebina, N., Gamo, T., Sano, Y., *et al*., 2015. Chemical composition of hydrothermal fluids in the central and southern Mariana Trough backarc basin. *Deep Sea Research Part II: Topical Studies in Oceanography*, **121**: 126-136.

Kamenetsky, V. S., Crawford, A. J., and Meffre, S., 2001. Factors controlling chemistry of magmatic spinel: An empirical study of associated olivine, Cr-spinel and melt inclusions from primitive rocks. *Journal of Petrology*, **42** (4): 655-671.

Kato, T., Beavan, J., Matsushima, T., Kotake, Y., Camacho, J. T., and Nakao, S., 2003. Geodetic evidence of back-arc spreading in the Mariana Trough. *Geophysical Research Letters*, **30** (12): 1625, DOI: 10.1029/2002GL016757.

Lai, Z. Q., Zhao, G. T., Han, Z. Z., Huang, B., Li, M., Tian, L. Y., *et al*., 2018. The magma plumbing system in the Mariana Trough back-arc basin at 18˚N. *Journal of Marine Systems*, **180**: 132-139.

Lambart, S., Laporte, D., and Schiano, P., 2013. Markers of the pyroxenite contribution in the major-element compositions of oceanic basalts: Review of the experimental constraints. *Lithos*, **160-161**: 14-36.

Le Bas, M. J., Le Maitre, R. W., Streckeisen, A., Zanettin, B., and IUGS Subcommission on the Systematics of Igneous Rocks, 1986. A chemical classification of volcanic rocks based on the total alkali-silica diagram. *Journal of Petrology*, **27** (3): 745-750.

Le Roux, V., Lee, C. T. A., and Turner, S. J., 2010. Zn/Fe systematics in mafic and ultramafic systems: Implications for detecting major element heterogeneities in the Earth's mantle. *Geochimica et Cosmochimica Acta*, **74** (9): 2779-2796.

Lee, C. T. A., Luffi, P., Plank, T., Dalton, H., and Leeman, W. P., 2009. Constraints on the depths and temperatures of basaltic magma generation on Earth and other terrestrial planets using new thermobarometers for mafic magmas. *Earth and Planetary Science Letters*, **279** (1-2): 20-33.

Li, H. Y., Li, X., Ryan, J. G., Zhang, C., and Xu, Y. G., 2022. Boron isotopes in boninites document rapid changes in slab inputs during subduction initiation. *Nature Communications*, **13** (1): 993.

Li, H. Y., Zhao, R. P., Li, J., Tamura, Y., Spencer, C., Stern, R. J., *et al*., 2021b. Molybdenum isotopes unmask slab dehydration and melting beneath the Mariana arc. *Nature Communications*, **12** (1): 6015.

Li, H., Arculus, R. J., Ishizuka, O., Hickey-Vargas, R., Yogodzinski, G. M., McCarthy, A., *et al*., 2021a. Basalt derived from highly refractory mantle sources during early Izu-Bonin-Mariana arc development. *Nature Communications*, **12** (1): 1723.

Li, X. H., Yan, Q. S., Zeng, Z. G., Fan, J., Li, S. Z., Li, J. J., *et al*., 2021c. Across-arc variations in Mo isotopes and implications for subducted oceanic crust in the source of back-arc basin volcanic rocks. *Geology*, **49** (10): 1165-1170.

Liu, Y. S., Gao, S., Kelemen, P. B., and Xu, W. L., 2008. Recycled crust controls contrasting source compositions of Mesozoic and Cenozoic basalts in the North China Craton. *Geochimica et Cosmochimica Acta*, **72** (9): 2349-2376.

Mariita, N. O., and Keller, G. R., 2007. An integrated geophysical study of the northern Kenya rift. *Journal of African Earth Sciences*, **48** (2): 80-94.

Masuda, H., and Fryer, P., 2015. Geochemical characteristics of active backarc basin volcanism at the southern end of the Mariana Trough. In: *Subseafloor Biosphere Linked to Hydrothermal Systems*. Ishibashi, J. I., *et al*., eds., Springer, New York, 261-273, DOI: 10.1007/978-4-431-54865-2_21.

Nekrylov, N., Portnyagin, M. V., Kamenetsky, V. S., Mironov, N. L., Churikova, T. G., Plechov, P. Y., *et al*., 2018. Chromium spinel in late Quaternary volcanic rocks from Kamchatka: Implications for spatial compositional variability of subarc mantle and its oxidation state. *Lithos*, **322**: 212-224.

Niu, Y. L., and O'Hara, M. J., 2003. Origin of ocean island basalts: A new perspective from petrology, geochemistry, and mineral physics considerations. *Journal of Geophysical Research*, **108** (B4): 2209, DOI: 10.1029/2002JB002048.

Ohara, Y., Stern, R. J., Ishii, T., Yurimoto, H., and Yamazaki, T., 2002. Peridotites from the Mariana Trough: First look at the mantle beneath an active back-arc basin. *Contributions to Mineralogy and Petrology*, **143** (1): 1-18.

Pearce, J. A., and Norry, M. J., 1979. Petrogenetic implications of Ti, Zr, Y, and Nb variations in volcanic rocks. *Contributions to Mineralogy and Petrology*, **69** (1): 33-47.

Pearce, J. A., Stern, R. J., Bloomer, S. H., and Fryer, P., 2005. Geochemical mapping of the Mariana arc-basin system: Implications for the nature and distribution of subduction components. *Geochemistry, Geophysics, Geosystems*, **6** (7): Q07006, DOI: 10.01029/02004GC000895.

Pertermann, M., and Hirschmann, M. M., 2003. Anhydrous partial melting experiments on MORB-like eclogite: Phase relations, phase compositions and mineral-melt partitioning of major elements at 2–3 GPa. *Journal of Petrology*, **44** (12): 2173-2201.

Plank, T., and Langmuir, C. H., 1998. The chemical composition of subducting sediment and its consequences for the crust and mantle. *Chemical Geology*, **145** (3): 325-394.

Putirka, K. D., Perfit, M., Ryerson, F. J., and Jackson, M. G., 2007. Ambient and excess mantle temperatures, olivine thermometry, and active *vs*. passive upwelling. *Chemical Geology*, **241** (3): 177-206.

Rüpke, L. H., Morgan, J. P., Hort, M., and Connolly, J. A. D., 2004. Serpentine and the subduction zone water cycle. *Earth and Planetary Science Letters*, **223** (1): 17-34.

Sano, Y., Nishio, Y., Gamo, T., Jambon, A., and Bernard, M., 1998. Noble gas and carbon isotopes in Mariana Trough basalt glasses. *Applied Geochemistry*, **13** (4): 441-449.

Scarrow, J. H., and Cox, K. G., 1995. Basalts generated by decompressive adiabatic melting of a mantle plume: A case study from the Isle of Skye, NW Scotland. *Journal of Petrology*, **36** (1): 3-22.

Sinton, J. M., and Fryer, P., 1987. Mariana Trough lavas from 18˚N: Implications for the origin of back arc basin basalts. *Journal of Geophysical Research: Solid Earth*, **92** (B12): 12782-12802.

Sobolev, A. V., Hofmann, A. W., Kuzmin, D. V., Yaxley, G. M.,

Arndt, N. T., Chung, S. L., *et al*., 2007. The amount of recycled crust in sources of mantle-derived melts. *Science*, **316** (5823): 412-417.

Sobolev, A. V., Hofmann, A. W., Sobolev, S. V., and Nikogosian, I. K., 2005. An olivine-free mantle source of Hawaiian shield basalts. *Nature*, **434** (7033): 590-597.

Stern, R. J., Bloomer, S. H., Martinez, F., Yamazaki, T., and Harrison, T. M., 1996. The composition of back-arc basin lower crust and upper mantle in the Mariana Trough: A first report. *Island Arc*, **5** (3): 354-372.

Stern, R. J., Fouch, M. J., and Klemerer, S. L., 2003, An overview of the Izu-Bonin-Mariana subduction factory. In: *Inside the Subduction Factory*. Eiler, J., ed., American Geophysical Union, Geophysical Monograph, Washington, D. C., 175-221.

Sun, S. S., and McDonough, W. F., 1989. Chemical and isotopic systematics of oceanic basalts: Implications for mantle composition and processes. *Geological Society, London, Special Publications*, **42** (1): 313-345.

Taylor, B., and Martinez, F., 2003. Back-arc basin basalt systematics. *Earth and Planetary Science Letters*, **210** (3-4): 481-497.

Tenzer, R., Bagherbandi, M., and Vajda, P., 2013. Global model of the upper mantle lateral density structure based on combining seismic and isostatic models. *Geosciences Journal*, **17** (1): 65-73.

Tian, L. Y., Zhao, G. T., Zhao, G. C., Shi, X. F., and Lv, H. L., 2010. Geochemistry of basaltic lavas from the Mariana Trough: Evidence for influence of subduction component on the generation of backarc basin magmas. *International Geology Review*, **47** (4): 387-397.

Volpe, A. M., Douglas Macdougall, J., and Hawkins, J. W., 1987. Mariana Trough basalts (MTB): Trace element and Sr-Nd isotopic evidence for mixing between MORB-like and arc-like melts. *Earth and Planetary Science Letters*, **82** (3): 241-254.

Wang, X. C., Li, Z. X., Li, X. H., Li, J., Liu, Y., Long, W. G., *et al*., 2012. Temperature, pressure, and composition of the mantle source region of late Cenozoic basalts in Hainan Island, SE Asia: A consequence of a young thermal mantle plume close to subduction zones? *Journal of Petrology*, **53** (1): 177-233.

Xu, Y., Yang, Y., Yu, H., Gao, W., Gao, X., Liu, B., *et al*., 2020. Geochemistry and petrogenesis of volcanic rocks from the continent-ocean transition zone in northern South China Sea and their tectonic implications. *Journal of Ocean University of China*, **19** (5): 1051-1061.

Yan, Q. S., Shi, X. F., Yuan, L., Yan, S. H., and Liu, Z. X., 2022. Tectono-magmatic evolution of the Philippine Sea Plate: A review. *Geosystems and Geoenvironment*, **1** (2): 100018.

Yan, Q. S., Zhang, P. Y., Metcalfe, I., Liu, Y. G., Wu, S. Y., and Shi, X. F., 2019. Geochemistry of axial lavas from the mid- and southern Mariana Trough, and implications for back-arc magmatic processes. *Mineralogy and Petrology*, **113** (6): 803-820.

Yang, Z. F., and Zhou, J. H., 2013. Can we identify source lithology of basalt? *Scientific Reports*, **3**: 1856.

Zhang, G. L., Zhang, J., Wang, S., and Zhao, J. X., 2020. Geochemical and chronological constraints on the mantle plume origin of the Caroline Plateau. *Chemical Geology*, **540**: 119566, DOI: 10.1016/j.chemgeo.2020.119566.

Zhang, G. L., Zong, C. L., Yin, X. B., and Li, H., 2012. Geochemical constraints on a mixed pyroxenite-peridotite source for East Pacific Rise basalts. *Chemical Geology*, **330-331**: 176-187.

Zhang, X., Zhai, S. K., Yu, Z. H., Guo, K., and Wang, S. J., 2019. Subduction contribution to the magma source of the Okinawa Trough–Evidence from boron isotopes. *Geological Journal*, **54**: 605-613.

Zhang, Y. X., Gazel, E., Gaetani, G. A., and Klein, F., 2021. Serpentinite-derived slab fluids control the oxidation state of the subarc mantle. *Science Advances*, **7** (48): eabj2515, DOI: 10.1126/sciadv.abj2515.

Zhao, G. T., Luo, W. Q., Lai, Z. Q., Tian, L. Y., and Xu, C. L., 2016. Influence of subduction components on magma composition in back-arc basins: A comparison between the Mariana and Okinawa Troughs. *Geological Journal*, **51** (S1): 357-367.

(Edited by Ji Dechun)